SCIENCE CHINA
Earth Sciences

• RESEARCH PAPER •
doi: 10.1007/s11430-014-5013-2

Energetics characteristics of the super magnetic storm on November 20, 2003 based on 3D global MHD simulation

HAN JinPeng[1,2*], WANG Chi[1] & LI Hui[1]

[1] *State Key Laboratory of Space Weather, Center for Space Science and Applied Research, Chinese Academy of Sciences, Beijing 100190, China;*
[2] *College of Earth Science, University of the Chinese Academy of Sciences, Beijing 100049, China*

Received June 30, 2014; accepted September 16, 2014

The three-dimensional global magnetohydrodynamic model (PPM-LR MHD) is employed to investigate the energy budget in the solar wind-magnetosphere system during the super magnetic storm on November 20, 2003, one of the biggest storms during the last decade with *Dst* ~ −500 nT. During this event, about 23% solar wind kinetic energy is transferred into the magnetosphere. The total energy input is estimated to be about 9.50×10^{17} J, about 14 times of a moderate storm. The energy dissipation via the inner magnetosphere is less than the energy input with the coupling efficiency of ~63.3%. The energy dissipated via ring current injection is less than that via high-latitude ionosphere at the initial stage of the super storm. Furthermore, both the simulation results and the empirical results indicate that the ratio of ring current injection to the total energy output increases with the enhancement of the magnetospheric activity level. These are consistent with the statistical results we have got before. The empirical equations underestimate the solar wind kinetic energy, the energy input, and the energy dissipation via high-latitude ionosphere compared with the simulation results; however, the coupling efficiency of the high-latitude ionosphere (23.4%) is close to the simulation result (23.1%) during the entire storm time period.

MHD simulation, energy budget, super storm, energy coupling function

Citation: Han J P, Wang C, Li H. 2014. Energetics characteristics of the super magnetic storm on November 20, 2003 based on 3D global MHD simulation. Science China: Earth Sciences, doi: 10.1007/s11430-014-5013-2

Estimating, modeling, and predicting energy transmission, conversion, and dissipation in the coupled solar wind-magnetosphere-ionosphere (SW-M-I) system are not only important for our basic understanding of the near-Earth environment activities but also meaningful for space weather purposes. For example, atmospheric heating during geomagnetic storms has a strong effect on satellite tracking, orbital decay, and orbital collision avoidance. With the growing interest in space weather activities during the past decades, the study of the magnetospheric energetics during geomagnetic storm or substorm has drawn more and more attention and become a major aspect of the investigation on storm-time energetics of the SW-M-I coupling system.

Geomagnetic storms are the large-scale disturbances in the Earth's magnetic field caused by enhanced solar wind-magnetosphere (SW-M) coupling processes. The ultimate source of magnetospheric energy is the solar wind. The estimation of energy transferred from the solar wind into the magnetosphere is the first step for the energetics research. The energy input process is closely related to the orientation of the interplanetary magnetic field (IMF). Most of the energy transferred into the magnetosphere is generally regarded as the consequence of the magnetic reconnection between the interplanetary magnetic field (IMF) and the Earth's magnetic field (Dungey, 1961). The estimation of the energy input into the magnetosphere can be conducted by the empirical coupling functions derived in many previ-

*Corresponding author (email: hanjp@spaceweather.ac.cn)

© Science China Press and Springer-Verlag Berlin Heidelberg 2014

ous studies from solar wind measurements (Akasofu, 1981; Finch and Lockwood, 2007; Newell et al., 2007; Perreault and Akasofu, 1978; Vasyliunas et al., 1982) (see Gonzalez (1990) for a review). The most popular one is the ε parameter derived by Akasofu (1981)

$$E_{\varepsilon}\left(\mathrm{W}\right)=\frac{4\pi}{\mu_0}VB^2\sin^4\left(\frac{\theta}{2}\right)l_0^2, \quad (1)$$

where V is the solar wind velocity, B is the IMF magnitude, θ is the IMF clock angle ($\tan\theta=B_y/B_z$), and l_0 is an empirical scaling factor denoting the linear dimension of the "effective cross-sectional area" of the SW-M interaction, which is usually assumed to be 7 R_E (Earth radii) (Akasofu, 1981; Perreault and Akasofu, 1978).

In fact, a number of coupling functions based on different data sets and approaches have emerged (Kan and Lee, 1979; Scurry and Russell, 1991; Temerin and Li, 2006; Wygant et al., 1983) during last a few decades. However, these coupling functions can only describe the energy input qualitatively. Most recently, on the basis of the dimensional analysis (Vasyliunas et al., 1982) and global MHD simulations, Wang et al. (2014) derived a new energy coupling function E_{in}, which can calculate the energy input quantitatively similar to ε parameter, shown as

$$E_{\mathrm{in}}\left(\mathrm{W}\right)=3.78\times10^7 n^{0.24}V^{1.47}B_T^{0.86}\left[\sin^{2.70}\left(\frac{\theta}{2}\right)+0.25\right], \quad (2)$$

where n is the number density in cm^{-3}, V is the velocity in km/s, and B_T is the IMF intensity in nT. This energy coupling function is suitable for a wide range of solar wind conditions and could be applied as an alternative means of the global MHD simulations.

Since the empirical energy coupling functions have been developed, the estimation of the energy sinks in the inner magnetosphere, such as the ring current and the high-latitude ionosphere, have evolved significantly. The Joule heating estimations were based mostly on ground magnetic measurements whereas estimations for the electron precipitation were based on both radar and spacecraft measurements. However, there is still a challenge to monitor the two energy dissipation processes on a global scale accurately. Several empirical formulas have been developed with the observation data (Ahn et al., 1983; Ahn et al., 1989; Akasofu, 1981; Baumjohann and Kamide, 1984; Cooper et al., 1995; Knipp et al., 2004; Lu et al., 1995; Østgaard et al., 2002a; Østgaard et al., 2002b; Richmond et al., 1990). Most of these empirical formulas used the AE or AL index to make the estimation. In addition to the inner magnetosphere energy sinks, some other energy sinks, plasmoid escaping and plasma sheet heating, have been identified in the early 1980s with the observations collected by ISEE mission (Hones et al., 1984).

With these empirical formulas to estimate the energy input and energy dissipation, many studies about the magnetospheric energetics during the geomagnetic storms have been conducted in the recent decades (Baker et al., 2001; Feldstein et al., 2003; Gonzalez et al., 1989; Kalegaev, 2000; Karavaev et al., 2009; Koskinen and Tanskanen, 2002; Li et al., 2012; Lu et al., 1998; MacMahon and Gonzalez, 1997; Rawat et al., 2010; Rosenqvist et al., 2006; Turner et al., 2006; Vichare et al., 2005; Xu and Du, 2012). Some of these studies were case analyses and some were statistical studies. MacMahon and Gonzalez (1997) investigated the energetics of the magnetosphere during the main phase of magnetic super storms ($Dst < -240$ nT) using the ε parameter to estimate the energy input and the empirical equations derived by Akasofu (1981) to estimate the energy dissipated in ring current. They found that the energy dissipation via Joule heating in the auroral ionosphere was about half of the ring current energy injection during super storms, which contradicted the previous results that Joule heating was roughly twice that of the ring current injection. However, other studies argued that the ionospheric dissipation was dominant in the partition of the energy dissipation (Baker et al., 2001; Feldstein et al., 2003; Knipp et al., 2004; Lu et al., 1998). Rosenqvist et al. (2006) investigated the magnetospheric energy budget during a sequence of intense substorm-like geomagnetic activity in October 2003. The estimations of energy input and energy dissipation were based on the Cluster observations, the European Incoherent Scatter (EISCAT), and the assimilated mapping of ionospheric electrodynamics (AMIE) technique. The results indicated that about 30% energy transferred into the magnetosphere was dissipated via Joule heating larger than the corresponding ratio (3%) based on empirical estimation. And they concluded that empirical proxies overestimated the energy input and underestimated Joule heating under extreme circumstances. Karavaev et al. (2009) calculated the ring current injection and ionospheric energy dissipation by using magnetogram inversion technique MIT-2 during the super storm on November 20, 2003. The results contradicted the dominant opinion that the energy input into the magnetosphere during disturbances was dissipated primarily in the ionosphere. They found that the ratio of ring current injection to the ionospheric energy dissipation would slowly increase with increasing activity level.

Rawat et al. (2010) investigated the energy budget of 18 intense geomagnetic storms and studied the effect of post-shock duration and magnitude of southward B_Z on the strength of the geomagnetic storms. They found that the southward directed magnitude and post-shock duration of IMF B_Z were important for causing big storms and that the high solar wind dynamic pressure with steady southward IMF B_Z could enhance the ring current energy and stimulate severe geomagnetic storm. In addition, many other statistical studies were focused mainly on the discrepancies caused by different driving sources, such as corotating interaction regions (CIRs), coronal mass ejections (CMEs), and sheath regions. Different activities on the Sun correspond to different interplanetary structures. The two major interplanetary drivers for causing intense geomagnetic storms are magnetic clouds (MCs) and sheath region behind the interplanetary shocks. Guo et al. (2011) investigated the differences of the energetics between the storms driven by CME and by CIR. Turner et al. (2009) studied the energy partitioning in CIR-driven and CME-driven storms and found that the coupling efficiency for the CIR-driven storms was larger than that for the CME-driven storms. Li et al. (2012) performed a statistical survey of 307 geomagnetic storms between 1995 and 2009 to investigate the magnetospheric energetics during magnetic storms. They found that the partition of the energy dissipation via ring current and high-latitude ionosphere was controlled by the storm intensity, the proportion of the ring current injection increased with the increase of the storm intensity, and the total energy input during the main phase was proportional to the storm intensity.

The previous studies on the energetics of the magnetosphere during geomagnetic storms were all based on the empirical equations, such as the ε parameter. However, the ε parameter was derived by fixing the energy input to equal the energy dissipation in the inner magnetosphere. Meanwhile, the energy input calculated from ε parameter represented the Poynting flux without including the mechanical energy. Therefore, the ε parameter underestimates the total energy input to some extent. In this study, we use a global MHD simulation model, PPMLR-MHD, to investigate the energetics characteristics of the magnetosphere during a super geomagnetic storm caused by an MC event on November 20, 2003.

1 Methodology

In this study, the global 3D Piecewise Parabolic Method with a Lagrangian Remap (PPMLR) MHD model developed by Hu et al. (2005) and Hu et al. (2007) is applied to simulate the geomagnetic storm and calculate the energy input into the magnetosphere. In addition, an empirical energy coupling function, the widely-used ε parameter (Akasofu, 1981), is also used to calculate the energy input for comparison. The energy dissipation in the high-latitude ionosphere is calculated by empirical formulas and MHD simulation and the energy dissipated by the ring current is calculated with empirical formula which is widely used and accepted for involving some difficulties in the MHD simulations.

1.1 PPMLR-MHD model

PPMLR-MHD model was developed by Hu et al. (2005) and Hu et al. (2007) to investigate the SW-M-I coupling processes. This code has been used in many previous studies, for example, the interaction of the interplanetary shocks with the magnetosphere, large-scale current systems (Wang et al., 2011), and Kelvin-Helmholtz (K-H) instabilities at the magnetopause (Wang et al., 2013). It is of three-order spatial precision and two-order temporal precision with small numerical dissipation. The solution domain of the code extends from −300 to 30 R_E in X direction and from −150 to 150 R_E in the Y and Z direction in GSM coordinate system and it is divided into 160×162×162 grid points: a uniform mesh is applied in the near-Earth domain of 0 R_E < $|X, Y, Z|$ < 10 R_E with a mesh grid 0.4 R_E, and the grid spacing outside increases according to a geometrical series of common ratio 1.05 along each axis. An inner boundary is set to be 3 R_E to avoid the complexity associated with the plasmasphere and the strong magnetic field. Two models developed by Moen and Brekke (1993) and Ahn et al. (1998) are used to determine the ionospheric Hall and Pedersen conductance contributed from the solar EUV radiation and the particle precipitation. The Hall and Pedersen conductance thus obtained are time-varying and non-uniform. In the SW-M system the MHD equations are conservative form which guarantee that energy, mass, and momentum are conserved in the simulation. The code solves the electrostatic equations in the high-latitude ionosphere domain. Other details can be found in Hu et al. (2007).

1.2 Energy input

In the past few decades, many studies on the solar wind energy transferred into the magnetosphere have been done and many coupling functions have been developed to describe the energy input process qualitatively. Most of the coupling functions were obtained empirically. At present, there are no direct observational means to determine the energy input into the magnetosphere. Global MHD simulations provide an effective approach to examine the global energy flow into the SW-M-I coupling system (Papadopoulos et al., 1999). Palmroth et al. (2003) simulated the energy flow from the solar wind to the magnetosphere during a major storm by using the global 3D MHD model, GUMICS-4 and developed streamline method to determine the magnetopause and the energy input. In this study, we use the streamline method to identify the magnetopause surface and calculate the energy input with higher resolution and more streamlines than that in Palmroth et al. (2003) until X= −60 R_E. More details about the improved streamline method can be found in the work of Wang et al. (2014).

Once the magnetopause surface is identified, the energy input through the surface can be calculated. The total input energy is defined as

$$E_{\mathrm{MHD}} = \int \boldsymbol{K} \cdot \hat{n} \mathrm{d}A, \tag{3}$$

where dA is the area of the surface element and $\hat{n}$ is the unit normal vector. $\boldsymbol{K}$ is the total energy flux, defined as

$$\boldsymbol{K}=\left(U+P-\frac{B^2}{2\mu_0}\right)\boldsymbol{V}+\frac{1}{\mu_0}\boldsymbol{E}\times\boldsymbol{B}\,, \tag{4}$$

where $U=P/(\gamma-1)+\rho V^2/2+B^2/(2\mu_0)$ is the total energy density including thermal energy density, kinetic energy density, and magnetic energy density, $\gamma=5/3$ is polytropic exponent, P is the thermal pressure, B is the magnetic field, $\boldsymbol{V}$ is the solar wind velocity, and $\boldsymbol{E}=-\boldsymbol{V}\times\boldsymbol{B}$ is the convectional electric field. $\boldsymbol{K}$ is interpolated from the PPMLR-MHD simulation at the center of each surface element with the vertices of the surface element.

In addition, the kinetic energy of the solar wind impinging on the dayside magnetopause per unit time can be calculated as

$$E_{\mathrm{SW}}=\frac{1}{2}\rho V_{\mathrm{SW}}^3 A\,, \tag{5}$$

where ρ and V_{SW} are the mass density and bulk velocity of the solar wind, respectively, and A is the cross section of the dayside magnetopause. Many different values of the cross section have been used in previous studies. Lu et al. (1998) suggested the cross section along the dawn-dusk meridian of the magnetopause, which is given by $\pi(r_0\times2^{\alpha})^2$. r_0 and α can be determined by Shue-98 magnetopause model (Shue et al., 1998), which represent the standoff distance at the subsolar point and the level of the tail flaring, respectively. In this study, we determine the cross section to be the maximum cross section of the magnetopause surface defined by streamline method.

1.3 Energy dissipation

1.3.1 Ring current injection

The ring current is an important channel to dissipate energy transferred into the magnetosphere. Since the MHD simulation involves some difficulties in calculating the energy dissipation in ring current, we determine the ring current energy dissipation by empirical formula. The ring current growth and decay, characterized by the *Dst* index, has been studied for thirty years using the equation of Burton et al. (1975). The original formula was based on the restriction of the Dessler-Parker-Sckopke (DPS) relation (Dessler and Parker, 1959; Sckopke, 1966) describing the relationship between *Dst* index and the energy of the ring current particles, which was widely accepted. In this study, we use this formula to calculate the ring current injection with *Dst* index. However, the *Dst* index has several other current sources except the ring current such as the dayside magnetopause current, the cross-tail current, and the ground-induced currents (see Maltsev (2004) for more details). Therefore, the effect of these additional current sources should be removed first from the measured *Dst* index in estimating the ring current injection. We use a dynamic pressure corrected method developed by Burton et al. (1975) to remove the effect of the magnetopause current shown as

$$Dst^*=Dst-b\sqrt{P_{\mathrm{d}}}+c\,, \tag{6}$$

where Dst^* is the pressure-corrected *Dst* index, and P_{d} is the solar wind dynamic pressure. Many studies have proposed various values of the coefficients b and c according different models (Gonzalez et al., 1994; O'Brien and McPherron, 2000; Turner et al., 2001). In this study, we choose b=7.26 nT nPa$^{-1/2}$ and c=11.0 nT (O'Brien and McPherron, 2000). In addition, Turner et al. (2001) considered that the ground-induces current and the cross-tail currents contributed about 21% and 25% of the Dst^*, respectively. Hence, the contribution of the ring current accounts for about 54% (Dst^{**}) of the Dst^* similar with the treatment done by Li et al. (2012). Thus, the energy dissipated by the ring current can be calculated using the relationship derived by Akasofu (1981) after the correction to the *Dst* index. The formula is shown as

$$U_{\mathrm{RC}}(\mathrm{GW})=-4\times10^4\left(\frac{\partial Dst^{**}}{\partial t}+\frac{Dst^{**}}{\tau}\right), \tag{7}$$

where Dst^{**} is expressed in nT and τ is the ring current decay time given in seconds. Many studies have proposed different models for the ring current lifetime (τ) (Gonzalez, 1993; Lu et al., 1998; MacMahon and Gonzalez, 1997; O'Brien and McPherron, 2000; Prigancova and Feldstein, 1992; Valdivia et al., 1996; Xu and Du, 2010), and for a review see Feldstein (1992). Table 1 lists six typical models of the ring current decay time summarized by Li et al. (2012).

In this study, we use the SYM-H index instead of the hourly *Dst* index. The SYM-H index is the same as the *Dst* index with higher time resolution of 1 min which can give a more detailed evolution of the ring current energy. In

Table 1 Six typical models of the ring current decay time (τ)

Model	Decay time τ (h)	Reference
BM1975	7.7	Burton et al. (1975)
A1981	20 for $\varepsilon < 100$ GW 6 for $100 < \varepsilon < 500$ GW 3 for $500 < \varepsilon < 1000$ GW 1 for $1000 < \varepsilon < 5000$ GW 0.3 for $5000 < \varepsilon < 10000$ GW 0.2 for $\varepsilon > 10000$ GW	Akasofu (1981)
G1993	4 for $Dst \geqslant -50$ nT 2 for $-50 > Dst \geqslant -100$ nT 1 for $-100 > Dst \geqslant -200$ nT 0.5 for $-200 > Dst \geqslant -300$ nT 0.25 for $Dst < -300$ nT	Gonzalez (1993)
VS1996	12.5/(1.0-0.0012Dst)	Valdivia et al. (1996)
OM2000	2.40exp[9.74/(4.69+VB_S)]	O'Brien and McPherron (2000)
XD2010	1/(0.1+3.0 × $10^{-4}\varepsilon$[GW])	Xu and Du (2010)

addition, the G1993 model of the ring current decay time is applied in the empirical equation to estimate the energy dissipation in the ring current, which is the best model for considering the correlation coefficients between the total dissipated energy via the ring current injection during the total storm period and storm intensity tested by Li et al. (2012).

1.3.2 Ionosphere energy dissipation

Joule heating and electron precipitation are the two energy dissipation channels in the ionosphere and can be estimated with auroral indices or determined locally from the data provided by satellites or radars. There are some difficulties in monitoring the two energy dissipation processes on a global scale accurately in real time. However, MHD simulation is a very effective approach to investigate the ionospheric energy dissipation on global scale. Joule heating, calculated from the scalar product of the current and electric field, is used to describe the Ohmic production of heat. In the ionosphere MHD simulation, the Joule heating is calculated as

$$P_{\mathrm{JH}} = \int \boldsymbol{J} \cdot \boldsymbol{E} \mathrm{d}S = \int \Sigma_{\mathrm{P}} E^2 \mathrm{d}S, \tag{8}$$

where $\boldsymbol{J}=\Sigma_{\mathrm{P}}\boldsymbol{E}$ is the electric current density, $\boldsymbol{E}$ is the electric field imposed on the ionosphere, and $\mathrm{d}S$ is the area element in the spherical ionosphere surface. Many models have been proposed to investigate the relationship between the ionospheric conductance and the energy flux of the auroral electrons in the past decades. Here the ionospheric Pedersen and Hall conductance model developed by Robinson et al. (1987) is inverted to get the energy flux due to the auroral electrons precipitation. The model formulas are shown as

$$\bar{E} = \left(\frac{\Sigma_{\mathrm{H}}}{0.45 \Sigma_{\mathrm{P}}} \right)^{\frac{1}{0.85}}, \tag{9}$$

$$\Phi_{\mathrm{E}} = \left[\frac{\Sigma_{\mathrm{P}} \left(16 + \bar{E}^2 \right)}{40 \bar{E}} \right]^2, \tag{10}$$

where Σ_{P} and Σ_{H} are the Pedersen and Hall conductance, which are available from MHD simulation, respectively; $\bar{E}$ is the average energy of the auroral electron in keV and Φ_{E} is the energy flux in ergs/(cm^2 s). The energy dissipation by the auroral electron precipitation in the polar ionosphere is the integration of the energy flux across the whole high-latitude ionosphere spherical surface, $P_{\mathrm{A}}=\int\Phi_{\mathrm{E}}\mathrm{d}S$.

Besides the MHD simulation, several empirical relations have been developed to estimate the energy dissipation via high-latitude ionosphere in the literature (Ahn et al., 1983; Ahn et al., 1989; Akasofu, 1981; Baumjohann and Kamide, 1984; Cooper et al., 1995; Knipp et al., 2004; Lu et al., 1995; Lu et al., 1998; Østgaard et al., 2002a; Østgaard et al., 2002b; Richmond et al., 1990; Zhang et al., 2005). Akasofu (1981) used the *AE* index to estimate the global Joule heating rate (U_{J}) and electron precipitation (U_{A}) and assumed that U_{A} was half of U_{J}. Ahn et al. (1983) and Ahn et al. (1989) used the *AE* and *AL* index derived from 12 or 71 stations data sets to do the estimation. The compiled empirical global Joule heating (CEJH) model proposed by Zhang et al. (2005) is a very effective means to study Joule heating patterns, Joule heating power, and their variation with solar wind conditions, geomagnetic activities, and the solar EUV radiation. Østgaard et al. (2002a) and Østgaard et al. (2002b) derived two new empirical formulas using the observation data collected by the Polar Ionospheric X-ray Imaging Experiment (PIXIE) and the Ultraviolet Imager (UVI) on board the Polar satellite of seven substorm in 1997. The empirical equations are shown as

$$U_{\mathrm{J}}\left(\mathrm{GW}\right) = 0.54 \times AE + 1.8, \tag{11}$$

$$U_{\mathrm{A}}\left(\mathrm{GW}\right) = 2 \times \left(4.4\sqrt{AL} - 7.6\right). \tag{12}$$

We would use these two empirical formulas to estimate the Joule heating and the electron precipitation and compare the results with MHD simulation results in this study.

2 Super geomagnetic storm

The term of MC was introduced by Burlaga et al. (1981) to characterize the magnetic field and plasma signature of an interplanetary post-shock flow observed by five spacecraft separated over more than 30° in solar longitude between 0.9 and 2 AU. MCs are the interplanetary manifestation of magnetized plasma ejected from the solar surface, which are one of the sources of geomagnetic storms. MCs are the subset of interplanetary coronal mass ejections (ICMEs) characterized by a low β and coherent IMF rotations through a relatively large scale. Gosling et al. (1990) investigated the ICMEs from 1978 to 1982 and found that about 30% of the ICMEs were MCs. According to Burlaga (1991), MCs can be identified at 1 AU through the following criteria: (1) the magnetic field direction rotates through a large angle during a time-interval of the order of one day; and (2) the magnetic field strength inside an MC is higher than in the average solar wind; and (3) the temperature inside an MC is lower than average. Criteria (2) and (3) imply low plasma-β values for MCs (Klein and Burlaga, 1982).

According to the above criteria, we select the famous MC, which arrived at the dayside magnetopause on November 20, 2003 with forward shock and caused the super geomagnetic storm, one of the two greatest events in 1957–2003, as shown in Figure 1. The solar wind conditions of the super geomagnetic storm have been listed in Figure 1, including temperature of the solar wind plasma, β value, solar wind number density, the total magnitude of the IMF, magnetic field latitude angle (θ), clock angle of the IMF, *X*

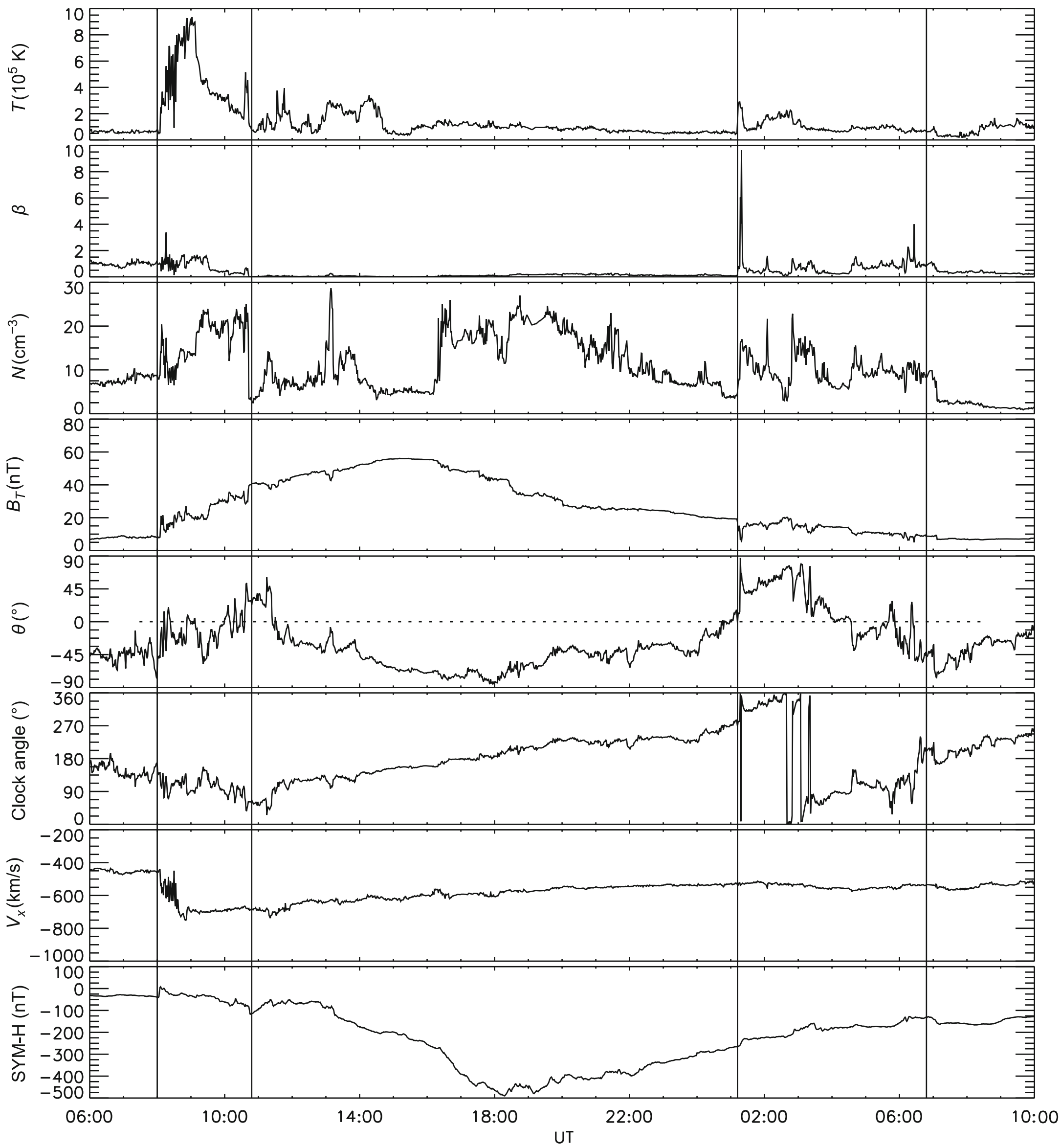

Figure 1 Solar wind conditions of the super geomagnetic storm caused by MC on November 20, 2003. The figure shows the plasma temperature, β value, number density, the total magnitude magnetic field, the latitude angle, the IMF clock angle, the x component velocity, and the SYM-H index from top to bottom. The first vertical line indicates the time when the forward shock arrives at the magnetosphere and the start time of the super storm, the second line is the main phase of the intense storm included in the super storm and the time of the arrival of the MC, the third line indicates the end time of the MC, and the fourth vertical line indicates the end of the recovery phase of the super storm.

component of the solar wind velocity, and SYM-H index obtained from the NASA OMNI database (http://omniweb.gsfc.nasa.gov/ow.html) from top to bottom .

It is very clear that the plasma temperature and β value both keep at a very low level for a long period, the magnitude of the IMF is very high and the clock angle changes from 60° to about 350°, and the magnetic field latitude angle changes from about 30° to −85° in main phase and then increases from −85° to 65° in recovery phase. The velocity of solar wind is larger than 600 km/s in storm time. These characteristics indicate a typical MC event.

In Figure 1, the first vertical line indicates the time when the forward shock arrives at the magnetosphere, which is characterized by the abrupt enhancement in solar wind velocity (V_{SW}) from 450 to 546 km/s, IMF intensity ($|B|$) from 8.2 nT to 15.4 nT, and solar wind density (N) from 8.8 to 14.2 cm^{-3}. The dynamic pressure (P_{SW}) increased from 3 to 8 nPa and further to 14 nPa (not shown). The forward shock causes the storm sudden commencement (SSC) of amplitude about 42 nT. The SSC lasts tens of minutes and then causes an intense geomagnetic storm (hereinafter intense storm) with the SYM-H index decreasing to −117 nT. During the initial period of the storm development, B_Z exhibits oscillating pattern but still is predominantly southward directed. The second vertical line indicates that the MC arrives at the magnetosphere characterized by the IMF magnitude increasing to 40 nT, solar wind velocity to 697 km/s, and the solar wind density decreasing from 18.4 to 3.5 cm^{-3} at 10:43 UT. Subsequently, the SYM-H index keeps decreasing to −490 nT, indicating a super geomagnetic storm at 18:17 UT (hereinafter super storm). The third vertical line indicates the end time of the MC with the temperature and β value increasing. The IMF turns to be northward. The β value is very low and the number density varies frequently between the second line time and the third line time. The intense storm starts at about 08:04 UT and ends at about 11:21 UT included in the super geomagnetic storm. The super geomagnetic storm ends at 06:50 UT November 21 marked by the fourth vertical line with the SYM-H increasing to 30% of the minimum SYM-H. The favorable magnetic field and solar wind conditions in the MC can accelerate the solar wind energy transfer process effectively due to significantly enhanced magnetic reconnection at the dayside magnetopause.

3 Results

In this study, a global 3D simulation model, PPMLR-MHD model, is applied to simulate the super geomagnetic storm caused by the famous MC on November 20, 2003 and the energetics characteristics of the magnetosphere are then investigated. The energy input and the energy dissipation in different region of the inner magnetosphere obtained from the MHD simulation are shown in Figure 2. The panels in Figure 2 from the top to the bottom are the energy input, the energy dissipation via ring current and high-latitude ionosphere, the energy budget of the magnetosphere, and the SYM-H index, respectively.

Before the arrival of the shock, the IMF intensity is less than 10 nT but the B_Z is still southward directed, which results in a small amount of the energy input from the solar wind into the magnetosphere. In this period, the average energy input power is about 2.46×10^{12} W. At the SSC of the storm, the energy input increases sharply to 9.90×10^{12} W since the forward shock arrives at the magnetosphere and compresses the magnetopause resulting in the earthward of the subsolar point and the increase of the SYM-H index. During the initial period of the storm, B_Z is oscillating but still southward directed. During the main phase of the intense storm, the average energy input is about 11.14×10^{12} W. However, the energy input decreases quickly to 2.15×10^{12} W at the end of the main phase of the intense storm for the decrease of the number density of solar wind and the turning northward of the IMF. In the recovery phase of the intense storm, the energy input increases gradually to 5.19×10^{12} W again and further rises to 10.12×10^{12} W with the increase of the solar wind number density at 11:33 UT.

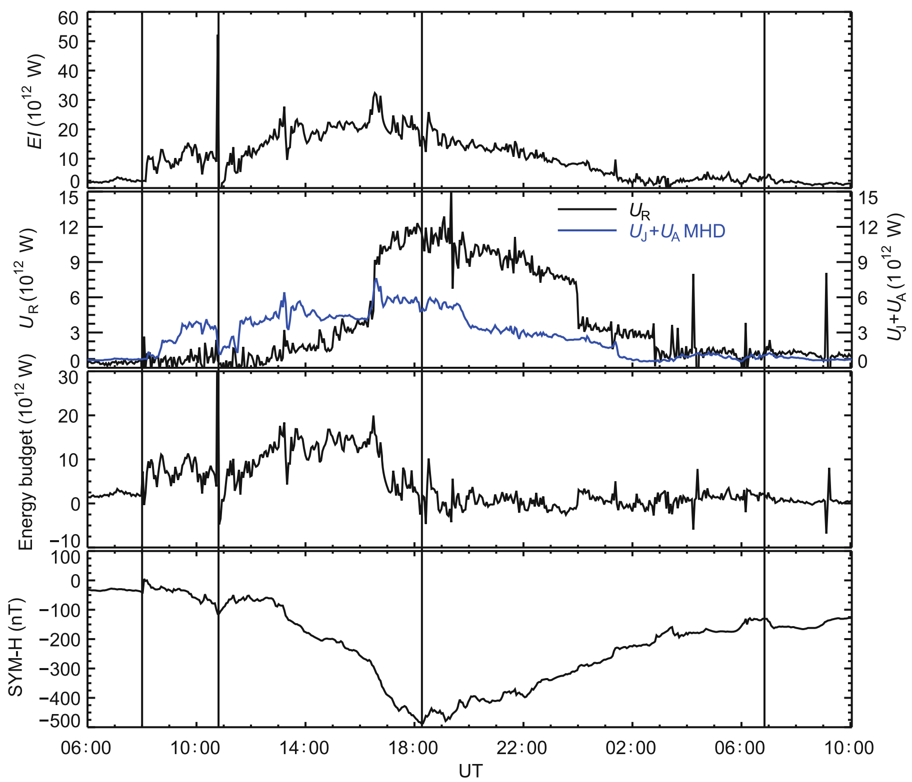

Figure 2 The energy input and dissipation of the geomagnetic storm obtained from the MHD simulation. From top to bottom, the figure shows the energy input, ring current energy dissipation and ionospheric energy dissipation, the energy budget, and the SYM-H index. The four vertical lines are the same as in Figure 1. The black line indicates the energy dissipation by the ring current and the blue line indicates the ionospheric energy dissipation in the second panel.

After the recovery phase, the SYM-H index remains stable of about −64 nT for one and a half hours and the energy input continues to increase to 20.2×10^{12} W at 12:51 UT and further rises to 27.7×10^{12} W at 13:13 UT. In the main phase of the super storm, the SYM-H decreases quickly and the energy input increases for the southward IMF and strong IMF magnitude. However, the deep of the solar wind number density results in the decrease of the energy input to 16.20×10^{12} W at 14:34 UT. And subsequently, the energy input increase slowly with the increase of the solar wind density, which implies that the solar wind number density plays an important role in the energy input process. At 18:17 UT the SYM-H decreases to the minimum value and starts to recover gradually. During the recovery phase of the super storm, the number density exhibits oscillating pattern and decreases gradually, the IMF intensity decrease slowly to 20 nT at the end time of MC, 01:16 UT November 21, and the direction of the IMF turns to be northward, which leads to the gradual decrease of the energy input.

The input efficiency (*IE*) in different period is also calculated to compare with the previous statistical study conducted by Li et al. (2012). The results of the input efficiency are listed in Table 2. The *IEs* in the intense storm are 13.2%, 9.0%, and 12.4%, respectively for main phase, recovery phase, and entire storm whereas the results in Li et al. (2012) for the same period are 11.8%, 4.3%, and 6.2%, respectively. The average results of the super storm including the first storm for the three period are 34.3%, 14.7%, and 23.3%, respectively, whereas the results are 33.8%, 8.3%, 14.7% in Li et al. (2012). The *IE* in main phase for both storms are consistent with Li et al. (2012) whereas in recovery phase the results in this study are larger than those in Li et al. (2012). This is because the results of Li et al. (2012) are obtained by using the ε parameter to determine the energy input. However, Koskinen and Tanskanen (2002) suggested that the ε parameter underestimates the energy input and a scaling parameter of 1.5–2 should be applied. Tenfjord and Østgaard (2013) considered that the ε parameter underestimated the energy input in the quiet period and overestimated the energy input under extreme conditions. Furthermore, the mechanical energy input is dominant under quiet conditions while the electromagnetic energy input is dominant under southward IMF conditions. And ε parameter is the first approximation of the electromagnetic energy input. Therefore, the underestimation level under quiet conditions such as recovery is more severe than that under southward IMF condition such as main phase. Thus, the different results between this study and Li et al. (2012) are expected.

Table 2 Comparison of the energy input efficiency (*IE*) results between this study and Li et al. (2012)[a)]

	Intense storm (%)	Super storm (%)
This study	(13.2, 9.0, 12.4)	(34.3, 14.7, 23.3)
Li et al. (2012)	(11.8, 4.3, 6.2)	(33.8, 8.3, 14.7)

a) The values in the bracket are for the main phase, the recovery phase, and the entire storm, respectively.

The second panel shows the variation of the energy dissipation in the ring current (the black solid line, U_{R}) and high-latitude ionosphere (the blue solid line, U_{iono}), respectively. Generally, both the energy dissipations via ring current injection and high-latitude ionosphere increase as the storm intensity increases. Before the SSC, there is a small amount of the energy input dissipated via ring current injection and high-latitude ionosphere. The average energy dissipation powers via ring current and high-latitude ionosphere are about 0.01×10^{12} W and 0.36×10^{12} W, respectively, in this period. After the arrival of the shock, the magnetosphere turns to be active and the average energy dissipation via ring current and high-latitude increases to 0.36×10^{12} W and 2.51×10^{12} W during the main phase of the intense storm and decreases to 0.21×10^{12} W and 1.67×10^{12} W during the recovery phase of the intense storm. At the end of the intense storm, the energy dissipation decreases sharply for the deep of the solar wind number density. During the stage of the super storm when the SYM-H drops rapidly, the energy dissipation via high-latitude maintains the high level and the energy dissipation via ring current injection rises gradually. At 16:25 UT, the sudden increase of the solar wind number density causes a great many of particles injecting into the ring current and the energy dissipation via ring current increases sharply to 10.42×10^{12} W at 16:51 UT and keeps at a high level for six hours. The energy dissipation decreases as the solar wind number density decreases and the energy dissipation via ring current injection exhibits oscillating pattern with the oscillation of the solar wind number density in this period. The total energy dissipations via ring current injection are 10.34×10^{16} J, 23.82×10^{16} J, and 34.23×10^{16} J for main phase, recovery phase, and entire super storm; 14.03×10^{16} J, 9.03×10^{16} J, and 23.11×10^{16} J for high-latitude ionosphere energy dissipation during the same stages.

The third panel shows the energy difference between the energy input into the magnetosphere and the total energy output in the ring current and high-latitude ionosphere. It is clear that the energy input is greater than the energy dissipation during the most time of the storm. An energy coupling efficiency (*CE*) was used by Turner et al. (2009) to represent the energy budget, which is defined as *CE* = (energy dissipation)/(energy input)×100%. When *CE* is less than 100%, which represents that the energy input is larger than energy dissipation, residual energy will be stored in the magnetosphere; when *CE* is greater than 100%, the magnetosphere will supply the energy sinks with the energy stored previously. The *CEs* of the energy sinks and the ratios of ring current injection and ionosphere energy dissipation to the total energy output during different stages of the storm are shown in Table 3. The *CE* is less than 100% during every phase of the storms, which indicates that there is a part of the energy input into the magnetosphere stored in the

Table 3 *CEs* of ring current and high-latitude ionosphere and the ratios of ring current and ionosphere energy dissipation to the total energy output during different stages of the storms[a)]

	Intense storm	Super storm
U_R	(0,33, 0.05, 0.38)	(10.34, 23.82, 34.23)
CE_R	(3.2, 0.63, 3.1)	(14.0, 61.3, 40.2)
Percentage (%)	(19.7, 21.7, 22.2)	(34.1, 71.3, 55.9)
U_{iono}	(2.30, 0.32, 2.67)	(14.03, 9.03, 23.11)
CE_{iono}	(24.4, 24.0,23.6)	(24.7, 21.9, 23.1)
Percentage (%)	(80.3, 77.3, 77.8)	(65.9, 28.7, 44.1)

a) Energies are expressed in 10^{16} J. The *CEs* and the ratios in the bracket are for the main phase, the recovery phase, and the entire storm.

magnetosphere to supply the energy in other magnetosphere activities or dissipated by other channels, such as plasma sheet heating. The ratio of the ring current is less than that of high-latitude in the initial period of the storm, which suggests that the energy is dissipated mainly in the high-latitude in the initial period of the storm. The amount of the energy dissipation via ring current increases gradually and the proportion of the ring current energy dissipation to the total energy output also increases with the increase of the magnetospheric activity level, which is consistent with the results of Li et al. (2012) and the conclusion of Karavaev et al. (2009), which calculated the ratio of the ring current energy dissipation to the high-latitude ionosphere energy dissipation to investigate the partition of the energy dissipation between the ring current injection and the high-latitude ionosphere dissipation. The average *CE* of ring current is about twice the average *CE* of high-latitude ionosphere during the entire super storm, which contradicts the previous results that Joule heating is roughly twice that of the ring current injection and is consistent with MacMahon and Gonzalez (1997). The average *CE* of the inner magnetosphere, ring current and high-latitude ionosphere, is about 63.3% which means that about 36.7% of the transferred energy into the magnetosphere is dissipated in other channels, such as plasma sheet heating and plasmoid ejection. The percentage of the energy dissipated in magnetotail is consistent with the result of Kamide and Baumjohann (1993).

4 Discussion

We investigate the energetics of the super geomagnetic storm caused by the MC event on November 20 using the global MHD simulation model, PPMLR-MHD. Besides the MHD simulation to determine the energy input, we also calculate the energy input using the widely used energy coupling function, ε parameter (Akasofu, 1981), to compare it with the simulation results. The results of the energy input from energy coupling functions are shown in Figure 3. The blue solid line is the results from the ε parameter, and the black solid line is the results from the MHD simulation. Overall, the blue line does not match well with the black line. During the intense storm, the ε parameter underestimates the energy input compared with the results from MHD simulation. During the main phase of the super storm, the intensity of the IMF increases to larger than 40 nT and the number density decreases to 5 cm^{-3} suddenly, which leads to the overestimation of ε. The overestimation of ε is due to the independence of the solar wind number density. This indicates that the solar wind number density affects the energy input process in the SW-M coupling system. During the recovery phase of the super storm, ε underestimates the energy input again compared with the MHD simulation. The correlation coefficient (*CC*) between the results from ε and the MHD simulation results and the prediction efficiency (*PE*) parameter, used to describe how the energy coupling function results are close to the simulation results, are calculated with *CC*=0.82 and *PE*=0.38.

In addition, the comparison of the energy dissipation via ionosphere between the simulation results and the empirical equation results is also conducted as shown in the middle panel of Figure 3. The energy dissipation from MHD simulation is greater than that from empirical equations, with an average ratio about 1.7. Although the results of the two methods are different, the time evolutions of the results match quite well to each other with a *CC* between the two methods results of 0.97. One reason of this discrepancy may lie in the fact that the empirical eqs. (11) and (12) were derived from the moderate storms and may not be applied to the super storm.

The comparisons between the empirical results and the MHD simulation results are summarized in Table 4. The solar wind kinetic energy is determined from eq. (5) and the cross areas are $\pi(r_0\times2^{\alpha})^2$ and the maximum cross section of the magnetopause surface for empirical method and MHD method, respectively. The empirical method underestimates the solar wind kinetic energy and the energy input compared with the simulation results. Although the energy magnitudes from the two methods are different, the variation trends of the energy partition between the ring current and the high-latitude ionosphere are similar for the two methods. The energy dissipation via ring current and the percentage of the ring current energy dissipation to the total energy output both increase with the increase of the magnetospheric activity level.

It is commonly accepted that the ionospheric conductances are controlled mainly by the solar EUV radiation, of which $F_{10.7}$ is a proxy, and the particle precipitation (Zhang et al., 2005). In our simulation, we used two models together to calculate the ionospheric Hall conductance and Pedersen conductance. An empirical model developed by Moen and Brekke (1993) is used to determine the contribution by the solar EUV radiation, which depends only on the solar flux $F_{10.7}$ and solar zenith angle χ:

$$\Sigma_{\mathrm{H}} = \left(F_{10.7}\right)^{0.53}\left(0.81\cos\chi + 0.54\cos^{1/2}\chi\right), \tag{13}$$

$$\Sigma_{\mathrm{P}} = \left(F_{10.7}\right)^{0.49}\left(0.34\cos\chi + 0.93\cos^{1/2}\chi\right). \tag{14}$$

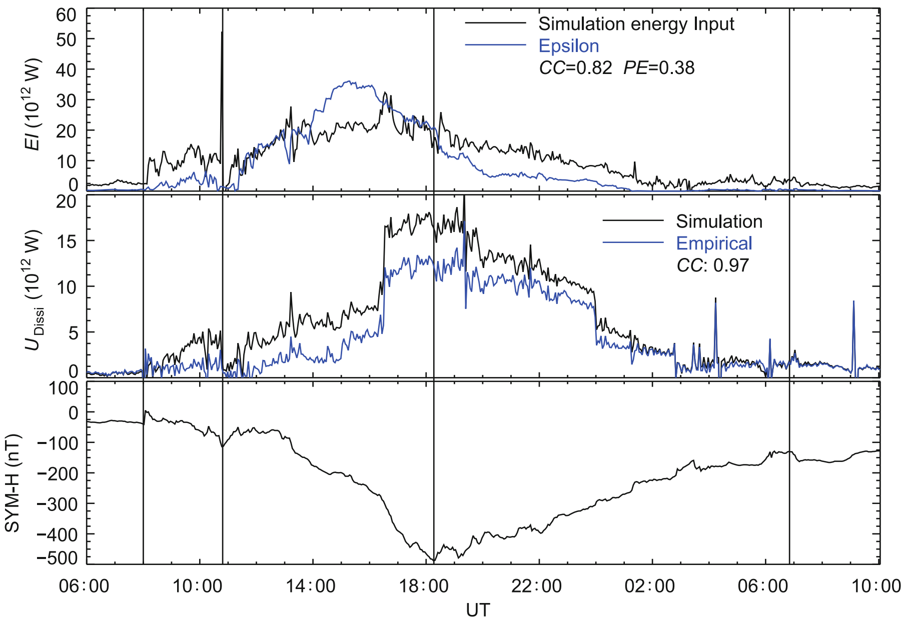

Figure 3 Comparisons of the energy input and energy dissipation between empirical results and MHD simulation results. The three panels are the comparison of the energy input, energy dissipation from MHD simulation with the results from empirical equations and the SYM-H index from top to bottom. The blue lines show the results of the empirical equations and the black lines represent the simulation results in the top two panels.

Table 4 Comparison of the results from empirical approaches and from MHD simulation[a)]

	Simulation results	Empirical results
E_{SW}	(243.40, 255.67, 506.76)	(171.16, 138.76, 313.21)
E_{in}	(58.62, 35.95, 95.03)	(61.49, 14.61, 76.51)
E_{Diss}	(24.37, 32.86, 57.34)	(13.72, 26.02, 39.89)
IE (%)	(34.3, 14.7, 23.3)	(49.8, 9.7, 27.2)
CE_R (%)	(14.0, 61.3, 40.2)	(17.5, 177.5, 82.7)
Percentage (%)	(34.1, 71.3, 55.9)	(51.0, 89.6, 71.9)
CE_{Iono} (%)	(24.7, 21.9, 23.1)	(26.8, 13.9, 23.4)
Percentage (%)	(65.9, 28.7, 44.1)	(49.0, 10.4, 28.1)

a) Energies are expressed in 10^{16} J. The values in the bracket are for the main phase, the recovery phase, and the entire storm of the super storm.

The other conductance model in our simulation is used for the auroral region with the geomagnetic disturbance data as follows:

$$\Sigma_{\mathrm{H,P}} = a \times \left|\Delta H\right|^{b} . \tag{15}$$

In this model, the auroral electrojets are divided into different region according to the combinations of the horizontal component and vertical component of the magnetic perturbation, as well as the magnetic local time (MLT). The formula is applied in each region with different values of a and b for different regions. The values of the constants are listed by Ahn et al. (1998). The Hall and Pedersen conductance thus obtained are time-varying and non-uniform.

In this study, the conductance model of Robinson et al. (1987) is inverted to calculate the energy flux of the precipitated particles (eqs. (9) and (10)) with the conductances contributed from the solar EUV radiation and the particle precipitation rather than with those only from the particle precipitation like in the original formula of Robinson et al. (1987). The treatment is for simplicity and acceptable for the most of the conductances are contributed from the particle precipitation and the solar EUV radiation only affects the dayside and low latitude region. The estimation indicates that this leads to about 14% overestimation of the particle precipitation energy dissipation. However, the high-latitude ionospheric energy dissipation is contributed mainly by the Joule heating, especially during the super geomagnetic storm. Therefore, the overestimation of the particle precipitation energy dissipation does not affect the results significantly. The distribution of the Hall and Pedersen conductance produced by the solar EUV radiation is shown in Figure 4.

5 Summary

In this study, the energetics of a super geomagnetic storm caused by the MC event on November 20, 2003 is investigated with global 3D MHD simulations. The MHD simulation provides an effective means to investigate the energetic of the magnetosphere during the storms for the absence of the observational means to determine the energy input. During this event, about 23% solar wind kinetic energy is transferred into the magnetosphere. The total energy input is estimated to be about 9.50×10^{17} J, about 14 times of a moderate storm. The *IE* is calculated with (13.2%, 9.0%, 12.4%) and (34.3%, 14.7%, 23.3%) of the intense storm and the super storm for the main phase, the recovery phase, and the entire storm, respectively. The *IEs* of the two storms during the main phase are consistent with the previous statistical

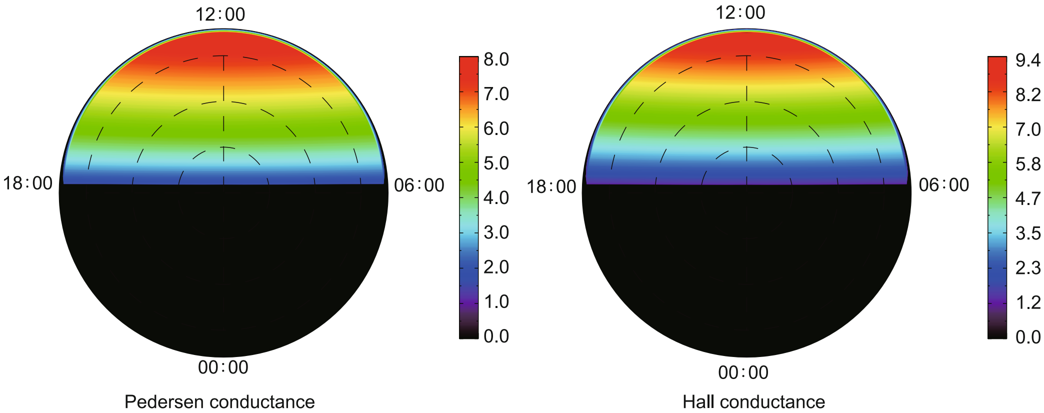

Figure 4 Distribution of the Pedersen conductance and Hall conductance produced by the solar EUV radiation. The solar EUV radiation affects the ionospheric conductances only in the dayside and low latitude region. The maximum conductances are in the 1200MLT and low latitude. The maximum values for Pedersen conductance and Hall conductance are 7.99 and 9.36, respectively, and are very small compared with the conductances produced by the particle precipitation during geomagnetic storms.

study conducted by Li et al. (2012). However, the *IEs* during the recovery phase in this study are larger than those in Li et al. (2012) for the ε underestimates the energy input during the recovery phase. The comparison between simulation results and ε results also indicates that the ε overestimates the energy input during the main phase when the solar wind number density decreases to a low level. This implies that the solar wind number density plays a very important role in the energy input process.

In addition, the average *CEs* of the storms for ring current injection and high-latitude ionosphere dissipation are also studied with 3.1%, 23.6% for intense storm and 40.2%, 23.1% for super storm. The partition of the energy dissipation via the ring current and high-latitude ionosphere varies with the intensity of the storms. Both the empirical results and the simulation results indicate that the proportion of the ring current injection to total energy output increases with the increase of the magnetospheric activity level. The energy dissipation via ring current injection is about twice of the energy dissipation via high-latitude ionosphere suggested by the simulation results. The simulation results also indicate that the energy budget between the energy input and the energy dissipation is unbalanced with about 63.3% of the transferred energy dissipated in the inner magnetosphere. This indirectly proves that the residual energy, about 36.7% of the transferred energy, is consumed by other energy dissipation channels in the tail, such as plasma sheet heating, plasmoid ejection returning to the solar wind, which is consistent with the previous study.

We wish to thank Binbin Tang of the State Key Laboratory of Space Weather, Center for Space Science and Applied Research, Chinese Academy of Sciences and Vladimir Mishin of the Institute of Solar-Terrestrial Physics of the Siberian Branch of the Russian Academy of Sciences, for their great help and useful discussions. The OMNI data were obtained from the GSFC/SPDF OMNI Web interface at http://omniweb.gsfc.nasa.gov. This work was supported by the National Basic Research Program of China (Grant No. 2012CB825602), the National Natural Science Foundation of China (Grant Nos. 41204118, 41231067), and the Specialized Research Fund for State Key Laboratories of China.

Ahn B H, Akasofu S I, Kamide Y. 1983. The Joule heat production rate and the particle energy injection rate as a function of the geomagnetic indices AE and AL. J Geophys Res-Space, 88: 6275–6287

Ahn B H, Kroehl H W, Kamide Y, et al. 1989. Estimation of ionospheric electrodynamic parameters using ionospheric conductance deduced from Bremsstrahlung X Ray image data. J Geophys Res-Space, 94: 2565–2586

Ahn B H, Richmond A D, Kamide Y, et al. 1998. An ionospheric conductance model based on ground magnetic disturbance data. J Geophys Res-Space, 103: 14769–14780

Akasofu S I. 1981. Energy coupling between the solar-wind and the magnetosphere. Space Sci Rev, 28: 121–190

Baker D N, Turner N E, Pulkkinen T I. 2001. Energy transport and dissipation in the magnetosphere during geomagnetic storms. J Atmos Sol-Terr Phy, 63: 421–429

Baumjohann W, Kamide Y. 1984. Hemispherical Joule heating and the AE indices. J Geophys Res-Space, 89: 383–388

Burlaga L F. 1991. Magnetic clouds. In: Schwenn R, Marsch E, eds. Physics of the Inner Heliosphere, Vol II. Heidelberg: Springer-Verlag. 1–22

Burlaga L F, Sittler E, Mariani F, et al. 1981. Magnetic loop behind an interplanetary shock: Voyager, Helios, and IMP 8 observations. J Geophys Res-Space, 86: 6673–6684

Burton R K, Mcpherron R L, Russell C T. 1975. An empirical relationship between interplanetary conditions and *Dst*. J Geophys Res-Space, 80: 4204–4214

Cooper M L, Clauer C R, Emery B A, et al. 1995. A storm time assimilative mapping of ionospheric electrodynamics analysis for the severe geomagnetic storm of November 8–9, 1991. J Geophys Res-Space, 100: 19329–19342

Dessler A J, Parker E N. 1959. Hydromagnetic theory of geomagnetic storms. J Geophys Res, 64: 2239–2252

Dungey J W. 1961. Interplanetary magnetic field and auroral zones. Phys Rev Lett, 6: 47–48

Feldstein Y I. 1992. Modelling of the magnetic field of magnetospheric ring current as a function of interplanetary medium parameters. Space Sci Rev, 59: 83–165

Feldstein Y I, Dremukhina L A, Levitin A E, et al. 2003. Energetics of the magnetosphere during the magnetic storm. J Atmos Sol-Terr Phy, 65: 429–446

Finch I, Lockwood M. 2007. Solar wind-magnetosphere coupling functions on timescales of 1 day to 1 year. Ann Geophys, 25: 495–506

Gonzalez W D. 1990. A unified view of solar wind-magnetosphere coupling functions. Planet Space Sci, 38: 627–632

Gonzalez W D. 1993. Ring current evolution during intense magnetic storms. Paper presented at Magnetic Storm/Substorm Relationship Workshop. Natl Geophys Data Cent, Breckenridge Colo, 24–27 June

Gonzalez W D, Tsurutani B T, Gonzalez A L C, et al. 1989. Solar wind-magnetosphere coupling during intense magnetic storms (1978–1979). J Geophys Res-Space, 94: 8835–8851

Gonzalez W D, Joselyn J A, Kamide Y, et al. 1994. What is a geomagnetic storm? J Geophys Res-Space, 99: 5771–5792

Gosling J T, Bame S J, Mccomas D J, et al. 1990. Coronal mass ejections and large geomagnetic storms. Geophys Res Lett, 17: 901–904

Guo J P, Feng X S, Emery B A, et al. 2011. Energy transfer during intense geomagnetic storms driven by interplanetary coronal mass ejections and their sheath regions. J Geophys Res-Space, 116: A05106

Hones E W, Pytte T, West H I. 1984. Associations of geomagnetic activity with plasma sheet thinning and expansion: A statistical study. J Geophys Res-Space, 89: 5471–5478

Hu Y Q, Guo X C, Wang C. 2007. On the ionospheric and reconnection potentials of the earth: Results from global MHD simulations. J Geophys Res-Space, 112: A07215

Hu Y Q, Guo X C, Li G Q, et al. 2005. Oscillation of quasi-steady Earth's magnetosphere. Chin Phys Lett, 22: 2723–2726

Kalegaev V V. 2000. Magnetospheric energy during magnetic storm on 23–27 November 1986. In: Wilson A, ed. Proceedings of the Fifth International Conference on Substorms. St. Petersburg, Russia: European Space Agency. 443–446

Kamide Y, Baumjohann W. 1993. Magnetosphere-Ionosphere Coupling. Heidelberg: Springer-Verlag. 177

Kan J R, Lee L C. 1979. Energy coupling function and solar wind-magnetosphere dynamo. Geophys Res Lett, 6: 577–580

Karavaev Y A, Sapronova L A, Bazarzhapov A D, et al. 2009. Energetics of the magnetospheric superstorm on November 20, 2003. Geomagn Aeron, 49: 961–969

Klein L W, Burlaga L F. 1982. Interplanetary magnetic clouds At 1 AU. J Geophys Res-Space, 87: 613–624

Knipp D J, Tobiska W K, Emery B A. 2004. Direct and indirect thermospheric heating sources for solar cycles 21–23. Sol Phys, 224: 495–505

Koskinen H E J, Tanskanen E I. 2002. Magnetospheric energy budget and the epsilon parameter. J Geophys Res-Space, 107: SMP 42-41–SMP 42-10

Li H, Wang C, Xu W Y, et al. 2012. Characteristics of magnetospheric energetics during geomagnetic storms. J Geophys Res-Space, 117: A04225

Lu G, Richmond A D, Emery B A, et al. 1995. Magnetosphere-ionosphere-thermosphere coupling: Effect of neutral winds on energy transfer and field-aligned current. J Geophys Res-Space, 100: 19643–19659

Lu G, Baker D N, McPherron R L, et al. 1998. Global energy deposition during January 1997 magnetic cloud event. J Geophys Res-Space, 103: 11685–11694

MacMahon R M, Gonzalez W D. 1997. Energetics during the main phase of geomagnetic superstorms. J Geophys Res-Space, 102: 14199–14207

Maltsev Y P. 2004. Points of controversy in the study of magnetic storms. Space Sci Rev, 110: 227–267

Moen J, Brekke A. 1993. The solar flux influence on quiet time conductances in the auroral ionosphere. Geophys Res Lett, 20: 971–974

Newell P T, Sotirelis T, Liou K, et al. 2007. A nearly universal solar wind-magnetosphere coupling function inferred from 10 magnetospheric state variables. J Geophys Res-Space, 112: A01206

O'Brien T P, McPherron R L. 2000. An empirical phase space analysis of ring current dynamics: Solar wind control of injection and decay. J Geophys Res-Space, 105: 7707–7719

Østgaard N, Vondrak R R, Gjerloev J W, et al. 2002a. A relation between the energy deposition by electron precipitation and geomagnetic indices during substorms. J Geophys Res-Space, 107: SMP 16-11–SMP 16-17

Østgaard N, Germany G, Stadsnes J, et al. 2002b. Energy analysis of substorms based on remote sensing techniques, solar wind measurements, and geomagnetic indices. J Geophys Res-Space, 107: SMP 9-1–SMP 9-14

Palmroth M, Pulkkinen T I, Janhunen P, et al. 2003. Stormtime energy transfer in global MHD simulation. J Geophys Res-Space, 108: 1048

Papadopoulos K, Goodrich C, Wiltberger M, et al. 1999. The physics of substorms as revealed by the ISTP. Phys Chem Earth Pt C, 24: 189–202

Perreault P, Akasofu S I. 1978. A study of geomagnetic storms. Geophys J Roy Astr S, 54: 547–573

Prigancova A, Feldstein Y I. 1992. Magnetospheric storm dynamics in terms of energy output rate. Planet Space Sci, 40: 581–588

Rawat R, Alex S, Lakhina G S. 2010. Storm-time characteristics of intense geomagnetic storms (*Dst* $\leqslant$–200 nT) at low-latitudes and associated energetics. J Atmos Sol-Terr Phy, 72: 1364-1371

Richmond A D, Kamide Y, Akasofu S I, et al. 1990. Global measures of ionospheric electrodynamic activity inferred from combined incoherent scatter radar and ground magnetometer observations. J Geophys Res-Space, 95: 1061–1071

Robinson R M, Vondrak R R, Miller K, et al. 1987. On calculating ionospheric conductances from the flux and energy of precipitating electrons. J Geophys Res-Space, 92: 2565–2569

Rosenqvist L, Buchert S, Opgenoorth H, et al. 2006. Magnetospheric energy budget during huge geomagnetic activity using Cluster and ground-based data. J Geophys Res-Space, 111: A10211

Sckopke N. 1966. A general relation between the energy of trapped particles and the disturbance field near the Earth. J Geophys Res, 71: 3125–3130

Scurry L, Russell C T. 1991. Proxy studies of energy transfer to the magnetosphere. J Geophys Res-Space, 96: 9541–9548

Shue J H, Song P, Russell C T, et al. 1998. Magnetopause location under extreme solar wind conditions. J Geophys Res-Space, 103: 17691–17700

Temerin M, Li X. 2006. *Dst* model for 1995–2002. J Geophys Res-Space, 111: A04221

Tenfjord P, Østgaard N. 2013. Energy transfer and flow in the solar wind-magnetosphere-ionosphere system: A new coupling function. J Geophys Res-Space, 118: 5659–5672

Turner N E, Mitchell E J, Knipp D J, et al. 2006. Energetics of magnetic storms driven by corotating interaction regions: A study of geoeffectiveness. In: Tsurutani B, McPherron R, Lu G, et al., eds. Recurrent Magnetic Storms: Corotating Solar Wind Streams. Washington D C: American Geophysical Union. 113–124

Turner N E, Cramer W D, Earles S K, et al. 2009. Geoefficiency and energy partitioning in CIR-driven and CME-driven storms. J Atmos Sol-Terr Phy, 71: 1023–1031

Turner N E, Baker D N, Pulkkinen T I, et al. 2001. Energy content in the storm time ring current. J Geophys Res-Space, 106: 19149–19156

Valdivia J A, Sharma A S, Papadopoulos K. 1996. Prediction of magnetic storms by nonlinear models. Geophys Res Lett, 23: 2899–2902

Vasyliunas V M, Kan J R, Siscoe G L, et al. 1982. Scaling relations governing magnetospheric energy transfer. Planet Space Sci, 30: 359–365

Vichare G, Alex S, Lakhina G S. 2005. Some characteristics of intense geomagnetic storms and their energy budget. J Geophys Res-Space, 110: A03204

Wang C, Zhang J J, Tang B B, et al. 2011. Comparison of equivalent current systems for the substorm event of 8 March 2008 derived from the global PPMLR-MHD model and the KRM algorithm. J Geophys Res-Space, 116: A07207

Wang C, Han J P, Li H, et al. 2014. Solar wind-magnetosphere energy coupling function fitting: Results from global MHD simulation. J Geophys Res-Space, 119: 6199–6212

Wang C, Guo X C, Peng Z, et al. 2013. Magnetohydrodynamics (MHD) numerical simulations on the interaction of the solar wind with the magnetosphere: A review. Sci China Earth Sci, 56: 1141–1157

Wygant J R, Torbert R B, Mozer F S. 1983. Comparison of S3-3 polar cap potential drops with the interplanetary magnetic field and models of magnetopause reconnection. J Geophys Res-Space, 88: 5727–5735

Xu W Y, Du A M. 2010. Effects of the ring current decay rate on the energy state of the magnetosphere. Chin J Geophys, 53: 1247–1255

Xu W Y, Du A M. 2012. Energy budget of the magnetosphere-ionosphere system in solar Cycle 23. Sci China Technol Sci, 55: 1184–1188

Zhang X X, Wang C, Chen T, et al. 2005. Global patterns of Joule heating in the high-latitude ionosphere. J Geophys Res-Space, 110: A12208